A MULTI-BAND TRANSCEIVER DESIGN FOR L/S/C-BAND TELEMETRY

Willie L. Thompson, II, D.Eng.
Morgan State University, The Clarence M. Mitchell, Jr. School of Engineering
Center of Excellence for Tactical and Advanced Communication Technologies (CETACT)

ABSTRACT

The Serial Streaming Telemetry infrastructure is being augmented with the Telemetry Network System, which is a net-centric infrastructure requiring bi-directional communications between the test article segment and the ground station segment. As a result, future radio segments must implement transceiver architecture to support bi-directional communications. This paper presents a design methodology for a multi-band transceiver design. The design methodology is based upon the Weaver architecture to provide coarse selection between the telemetry bands. Utilization of the Weaver architecture allowed for the optimization of multiple transmitter and receiver channels into single channels to support the L/S/C-Band frequency allocations. System-level simulation is presented to evaluate the feasibility of the transceiver design for a multi-band, multi-mode software-defined radio (SDR) platform in support of Telemetry Network System.

KEY WORDS

Multi-band Transceiver, RF Front End, Image Rejection Architecture, C-Band Telemetry

INTRODUCTION

The traditional telemetry infrastructure is a point-to-point communication system consisting of a transmitter located on a test article segment and a receiver located at the ground station segment. As a result, the communication system is an unidirectional link and is referred to as Serial Streaming Telemetry (SST). The SST infrastructure is being augmented with the Telemetry Network System (TmNS). The TmNS is a net-centric infrastructure requiring a bi-directional link between the test article segment and ground station segment. In the future, the SST infrastructure will be removed leaving a fully net-centric telemetry infrastructure. As a result, future radio segments must transition from transmitter/receiver architectures to transceiver architectures to support bi-directional communications.

In recent years, the aeronautical telemetry infrastructure is being challenged by a growing increase in the volume of telemetry data, while the downlink time has remained the same or decreased due to the dynamics of the test article segment. As a result, improvements in the data

rate performance of the telemetry infrastructure have become critical to support this new demand for telemetry data. However, the available RF spectrum has decreased due to the encroachment of the commercial wireless industry into the telemetry allocations, which adversely impacts the data rate performance. The data rate versus RF spectrum crisis must be address to support future telemetry applications. To meet these challenges, C-Band spectrum has been allocated for telemetry applications. Therefore, it would be advantageous that future radio segments support tri-band operation across the L/S/C-band telemetry allocations.

A future telemetry radio segment architecture based on a software-defined radio (SDR) platform is illustrated in Figure 1. The architecture consists of three sub-systems: multi-band front end with transmitter (Tx) and receiver (Rx) channels, the digital radio, and the configuration and control (C^2). The multi-band front end provides wideband operation, coarse band selection, and channel tuning that support L/S/C-band telemetry allocations. Coarse band selection utilizes the property of image rejection within the Weaver architecture to select between the L/S-band and C-band allocations, respectively [1]. The band selection capabilities of the Weaver architecture have been demonstrated in various applications [2-4]. The digital radio implements field-programmable gate array (FPGA) technology to provide high-speed signal processing and programmability to support multiple telemetry waveforms: Pulse Code Modulation/Frequency Modulation (PCM/FM) and Shaped Offset Quadrature Shift Keying (SOQPSK-TG). The C^2 sub-system allows for pre-test configuration and control of the multi-band front end and digital radio.

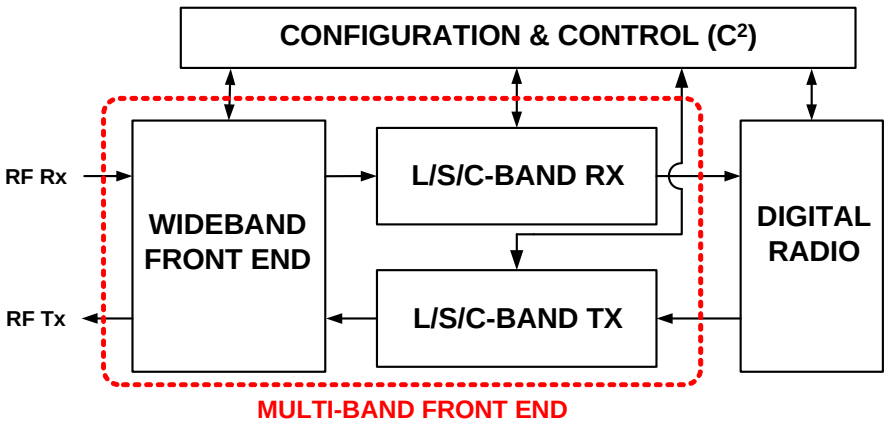

Figure 1: Future telemetry radio segment architecture

DESIGN METHODOLOGY

The design methodology for the multi-band transceiver design is based on the properties of frequency translation and image-rejection of the Weaver architecture. When frequency translation is performed, a lower sideband (LSB) component and an upper sideband (USB) component are generated. These two components will be located at equal distance from the local oscillator (LO) frequency and are referred to as image frequencies of each other. In typical applications, one of these sideband components would be retained and other component would be rejected. However, the property of the image frequencies can be used to provide coarse

selection between the L/S-band and C-band telemetry bands by properly selecting the LO frequencies and sideband component. The design methodology for the L/S/C-band transmitter (Tx) channel is illustrated in Figure 2.

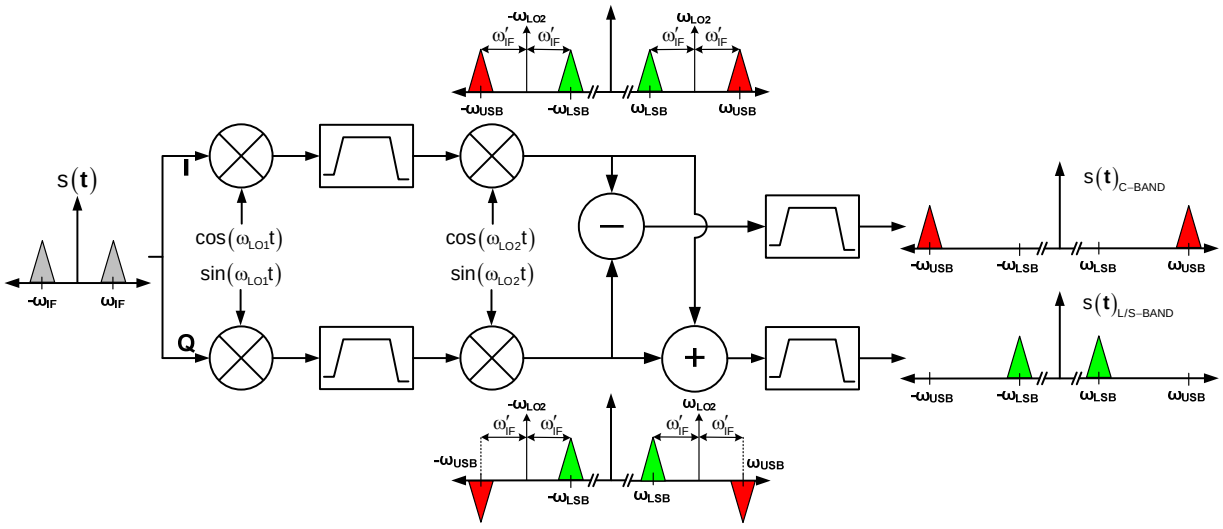

Figure 2: Design methodology for Tx channel

The Weaver architecture is a two-stage frequency translation architecture that generates the output spectrums for the in-phase (I) path and quadrature (Q) path as illustrated in Figure 2. For the Q path, the USB component has a 180-degree phase difference as compared to the I-path USB component. This phase difference can be used to select between sideband components. Assuming the input signal is:

$$s(t) = A\cos(\omega_{IF}t + \theta) \tag{1}$$

where A is the amplitude, ω_{IF} is the intermediate frequency in radians, and θ is the phase in radians of the modulated waveform. Performing the two-stage frequency translation for the I path, the expression for the USB component is:

$$\begin{aligned} s(t)_{I\_USB} &= s(t) \times \cos(\omega_{LO1}t) \times \cos(\omega_{LO2}t) \\ s(t)_{I\_USB} &= \tfrac{A}{4}\cos\left[(\omega_{LO2} + \omega'_{IF})t + \theta\right] \end{aligned} \tag{2}$$

where ω'_{IF} is the intermediate frequency between the first and second frequency translations after the band-pass filter. The expression for the LSB component for the I path is:

$$\begin{aligned} s(t)_{I\_LSB} &= s(t) \times \cos(\omega_{LO1}t) \times \cos(\omega_{LO2}t) \\ s(t)_{I\_LSB} &= \tfrac{A}{4}\cos\left[(\omega_{LO2} - \omega'_{IF})t + \theta\right] \end{aligned} \tag{3}$$

By properly selecting the $\omega_{IF}^{'}$ and the second LO frequency (ω_{LO2}), the USB component can generate the C-band telemetry frequencies and the LSB component can generate the L/S-band telemetry frequencies, respectively. The expressions for $\omega_{IF}^{'}$ and ω_{LO2} are:

$$\omega_{LO2} = \frac{\omega_{USB} + \omega_{LSB}}{2} \qquad \omega'_{IF} = \omega_{LO2} - \omega_{LSB}$$
$$\omega_{USB} = \frac{\omega_{C-Band\_UpperEdge} + \omega_{C-Band\_LowerEdge}}{2} \tag{4}$$
$$\omega_{LSB} = \frac{\omega_{L/S-Band\_UpperEdge} + \omega_{L/S-Band\_LowerEdge}}{2}$$

Performing the two-stage frequency translation for the Q path, the expression for the USB component is:

$$s(t)_{Q\_USB} = s(t) \times \sin(\omega_{LO1} t) \times \sin(\omega_{LO2} t)$$
$$s(t)_{Q\_USB} = -A/4 \cos\left[(\omega_{LO2} + \omega'_{IF})t + \theta\right] \tag{5}$$

And the expression of the LSB component for the Q path is:

$$s(t)_{Q\_LSB} = s(t) \times \sin(\omega_{LO1} t) \times \sin(\omega_{LO2} t)$$
$$s(t)_{Q\_LSB} = A/4 \cos\left[(\omega_{LO2} - \omega'_{IF})t + \theta\right] \tag{6}$$

To transmit within the C-band allocation, the difference of the I and Q paths is used. Using (2) - (6), the expression of the final output C-band allocation, which is the USB component, is:

$$s(t)_{C-BAND} = s(t)_{I\_USB} - s(t)_{Q\_USB}$$
$$s(t)_{C-BAND} = A/4 \cos\left[(\omega_{LO2} + \omega'_{IF})t + \theta\right] - \left\{-A/4 \cos\left[(\omega_{LO2} + \omega'_{IF})t + \theta\right]\right\} \tag{7}$$
$$s(t)_{C-BAND} = A/2 \cos\left[(\omega_{LO2} + \omega'_{IF})t + \theta\right]$$

and the output for L/S-band allocation, which is the LSB component, is:

$$s(t)_{L/S-BAND} = s(t)_{I\_LSB} - s(t)_{Q\_LSB}$$
$$s(t)_{L/S-BAND} = A/4 \cos\left[(\omega_{LO2} - \omega'_{IF})t + \theta\right] - A/4 \cos\left[(\omega_{LO2} - \omega'_{IF})t + \theta\right] \tag{8}$$
$$s(t)_{L/S-BAND} = 0 \leftarrow \text{ L/S-band allocation is suppressed}$$

As result, the output for the C-band allocation is selected and the L/S-band allocation is suppressed as illustrated in Figure 2. To transmit within the L/S-band allocation, the sum of the I and Q paths is used. Using (2) - (6), the expression of the final output L/S-band allocation, which is the LSB component, is:

$$
\begin{aligned}
s(t)_{L/S-BAND} &= s(t)_{I\_LSB} + s(t)_{Q\_LSB} \\
s(t)_{L/S-BAND} &= A/4 \cos\left[(\omega_{LO2} - \omega'_{IF})t + \theta\right] + A/4 \cos\left[(\omega_{LO2} - \omega'_{IF})t + \theta\right] \\
s(t)_{L/S-BAND} &= A/2 \cos\left[(\omega_{LO2} - \omega'_{IF})t + \theta\right]
\end{aligned} \tag{9}
$$

and the output for C-band allocation, which is the USB component, is:

$$
\begin{aligned}
s(t)_{C-BAND} &= s(t)_{I\_USB} + s(t)_{Q\_USB} \\
s(t)_{C-BAND} &= A/4 \cos\left[(\omega_{LO2} + \omega'_{IF})t + \theta\right] - A/4 \cos\left[(\omega_{LO2} + \omega'_{IF})t + \theta\right] \\
s(t)_{C-BAND} &= 0 \leftarrow \text{ C-band allocation is suppressed}
\end{aligned} \tag{10}
$$

As a result, the output for the L/S-band allocation is selected and the C-band allocation is suppressed as illustrated in Figure 2.

The design methodology for the L/S/C-band receiver (Rx) channel is illustrated in Figure 3. The critical design consideration is ensuring that the L/S-band and C-band allocations are image frequencies. By properly selecting the LO frequencies, the L/S-band allocation can be assigned as the LSB component, while the C-band allocation can be assigned as the USB component. Using (4), the first LO frequency (ω_{LO1}) must be:

$$
\omega_{LO1} = \frac{\omega_{USB} + \omega_{LSB}}{2} \tag{11}
$$

where ω_{LSB} is the center frequency of the L/S-band allocation and ω_{USB} is the center frequency of the C-band allocation. When performing frequency translation, these allocations will be translated to the same IF frequency. However, the Weaver architecture will generate a 180-degree phase difference in the Q path as illustrated in Figure 3. For the I path, the USB and LSB components are in phase with each other and is denoted by the yellow notation. For the Q path, the USB and LSB components are out of phase with each other and are denoted by with their appropriate color notation. The analytical analysis for the Rx channel is the same as the Tx channel given the following expressions for the USB and LSB signals:

$$
\begin{aligned}
r(t)_{USB} &= A\cos(\omega_{USB}t + \theta) \\
r(t)_{LSB} &= A\cos(\omega_{LSB}t + \theta)
\end{aligned} \tag{12}
$$

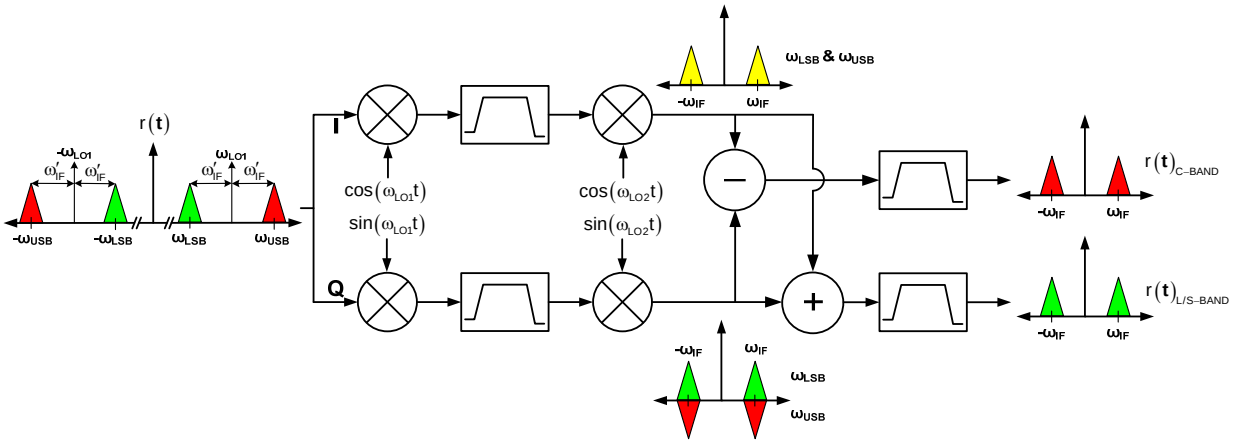

Figure 3: Design methodology for Rx channel

Performing the same analysis as in (2) - (10), the expression of the final output for C-band allocation, which is the USB component, is:

$$\begin{aligned} r(t)_{C-BAND} &= r(t)_{I\_USB} - r(t)_{Q\_USB} \\ r(t)_{C-BAND} &= \tfrac{A}{4}\cos\left[\left(\omega'_{IF} - \omega_{LO2}\right)t + \theta\right] - \left\{-\tfrac{A}{4}\cos\left[\left(\omega'_{IF} - \omega_{LO2}\right)t + \theta\right]\right\} \\ r(t)_{C-BAND} &= \tfrac{A}{4}\cos\left[\left(\omega'_{IF} - \omega_{LO2}\right)t + \theta\right] \end{aligned} \tag{13}$$

where ω'_{IF} is the intermediate frequency between the first and second frequency translations after the band-pass filter and is equal to:

$$\omega'_{IF} = \frac{\omega_{USB} - \omega_{LSB}}{2} \tag{14}$$

The output spectrum for L/S-band allocation, which is the LSB component, is:

$$\begin{aligned} r(t)_{L/S-BAND} &= r(t)_{I\_LSB} - r(t)_{Q\_LSB} \\ r(t)_{L/S-BAND} &= \tfrac{A}{4}\cos\left[\left(\omega'_{IF} - \omega_{LO2}\right)t + \theta\right] - \tfrac{A}{4}\cos\left[\left(\omega'_{IF} - \omega_{LO2}\right)t + \theta\right] \\ r(t)_{L/S-BAND} &= 0 \leftarrow \text{ L/S-band allocation is suppressed} \end{aligned} \tag{15}$$

Similarly, the expression of the output spectrum for L/S-band allocation is:

$$\begin{aligned} r(t)_{L/S-BAND} &= r(t)_{I\_LSB} + r(t)_{Q\_LSB} \\ r(t)_{L/S-BAND} &= \tfrac{A}{4}\cos\left[\left(\omega'_{IF} - \omega_{LO2}\right)t + \theta\right] + \tfrac{A}{4}\cos\left[\left(\omega'_{IF} - \omega_{LO2}\right)t + \theta\right] \\ r(t)_{L/S-BAND} &= \tfrac{A}{2}\cos\left[\left(\omega'_{IF} - \omega_{LO2}\right)t + \theta\right] \end{aligned} \tag{16}$$

and the output spectrum for C-band allocation:

$$
\begin{aligned}
r(t)_{C-BAND} &= r(t)_{I\_USB} + r(t)_{Q\_USB} \\
r(t)_{C-BAND} &= \tfrac{A}{4}\cos\left[\left(\omega'_{IF} - \omega_{LO2}\right)t + \theta\right] - \tfrac{A}{4}\cos\left[\left(\omega'_{IF} - \omega_{LO2}\right)t + \theta\right] \\
r(t)_{C-BAND} &= 0 \leftarrow \text{ C-band allocation is suppressed}
\end{aligned} \tag{17}
$$

FREQUENCY PLANNING

The telemetry frequency allocations are presented in Table 1. Currently, there are no system-level requirements to support simultaneous communications between the frequency allocation. As a result, there are four Tx/Rx configuration modes were analyzed as outlined in Table 2. The Tx channel has a single L/S-band allocation and two C-band allocations, while the Rx channel has two L/S-band allocations and a single C-band allocation.

Table 1: Tx/Rx Frequency Allocations [5]

Tx Frequency Allocations	Rx Frequency Allocations
S-Band: 2360 – 2395 MHz	L-Band: 1435 – 1535 MHz
C-Band: 4400 – 4940 MHz	S-Band: 2200 – 2290 MHz
C-Band: 5091 – 5150 MHz	C-Band: 4400 – 4940 MHz

For Tx modes, the ω_{LO2} ensures that the LSB and USB components are generated within the L/S-band and C-band allocations. Using (4), the required ω_{LO2} frequencies for the TX-I and TX-II modes are 3523.75 MHz and 3749 MHz, respectively. Conceptually, these frequencies are the mid-points between the two frequency allocations. Given an intermediate frequency (ω_{IF}), the first LO frequency can be calculated using the following expression:

$$\omega_{LO1} = \omega'_{IF} - \omega_{IF} = \omega_{LO2} - \omega_{LSB} - \omega_{IF} \tag{18}$$

Table 2: Tx/Rx Configuration Modes

Configuration Mode	LSB Allocation	USB Allocation
TX-I	S-Band: 2360 – 2395 MHz	C-Band: 4400 – 4940 MHz
TX-II	S-Band: 2360 – 2395 MHz	C-Band: 5091 – 5150 MHz
RX-I	L-Band: 1435 – 1535 MHz	C-Band: 4400 – 4940 MHz
RX-II	S-Band: 2200 – 2290 MHz	C-Band: 4400 – 4940 MHz

For Rx modes, the ω_{LO1} ensures that the L/S-band and C-band allocations are image frequencies. Using (11), the required ω_{LO1} frequencies for the RX-I and RX-II modes are 3077.5 MHz and 3457.5 MHz, respectively. Using (14), the second frequency translation provides ω_{IF} for demodulation by the digital radio and can be calculated using:

$$\omega_{LO2} = \omega'_{IF} - \omega_{IF} = \frac{\omega_{USB} - \omega_{LSB}}{2} - \omega_{IF} \tag{19}$$

Figure 4 presents the frequency planning for the Tx/Rx configuration modes.

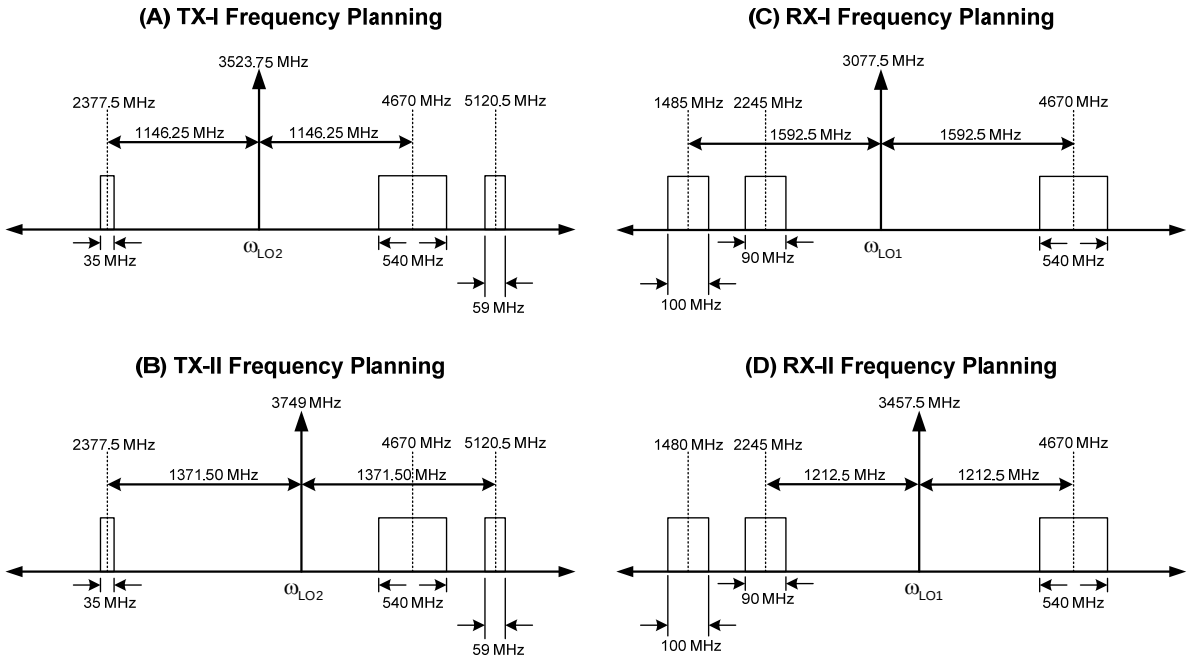

Figure 4: Tx/Rx Frequency Planning

DESIGN VERIFICATION

System-level simulations were performed as verification of the design methodology. Each of the Tx/Rx configuration modes was analyzed for feasible to perform coarse band selection utilizing the Weaver architecture as illustrated in Figure 2 andFigure 3. Simulation results for TX-I and RX-I configuration modes are presented in Figure 5. For the TX-I mode, the input signal was a 70-MHz single-tone signal. The sum output generated LSB component at 2377.5 MHz (S-Band) and the difference output generated USB component at 4670 MHz (C-Band). For the RX-I mode, the input signal was two-tones of 1-MHz LSB component at 1485 MHz (L-Band), and 2-MHz USB component at 4670 MHz (C-Band). Different bandwidths were used to denote the different sideband component that generated the 70-MHz signal. The sum output generated a 1-MHz component at 70-MHz from the LSB component, while the difference output generated a 2-MHz component at 70-MHz from the USB component.

A figure of merit for the ability to suppress the unwanted (image) sideband component is the image-rejection ratio (IRR). IRR is the ratio of the power level produced by the unwanted sideband component to the power level produced by the wanted sideband component. In Figure 5, the simulation results were based on ideal component performance result in IRR > 40 dB. However, the IRR degrades due to amplitude and phase imbalances between I and Q paths. For a 1-dB amplitude imbalance, simulations demonstrated an IRR of 27 dB, while for a 2-dB amplitude imbalance, the IRR degraded to 17 dB. Likewise, for phase imbalance of 1-degree and 2 degree, the IRR is 37 dB and 34 dB, respectively. As a result, compensation techniques should be implemented to improve I/Q imbalance [6] – [7].

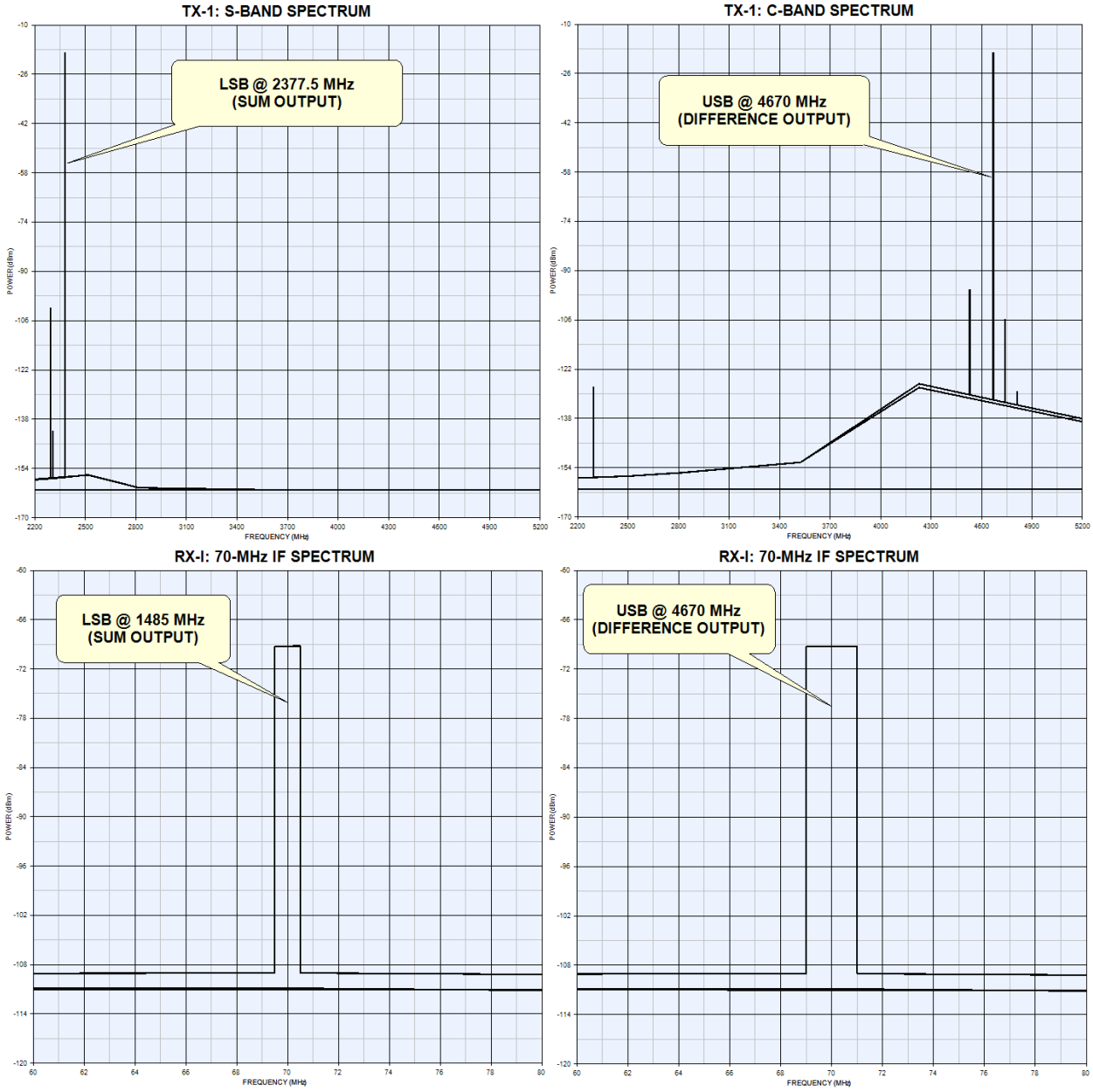

Figure 5: Simulation result for TX-I and RX-I modes

CONCLUSION

A design methodology for multi-band transceiver design was demonstrated through analytical formulation and system-level simulation. The multi-band transceiver design is optimized into single L/S/C-band Tx and Rx channels by utilizing the property of image rejection within the Weaver architecture to perform coarse selection between the L/S-band and C-band allocations, respectively. This work will serve as the foundational design methodology for the development of a multi-band, multi-mode SDR platform for next-generation L/S/C-band radio segment.

ACKNOWLEDGEMENTS

This work was funded under the Scientific Research Corporation/Morgan State University partnership in support of the Test Resource Management Center's Science & Technology Program for Spectrum Efficient Technology.

REFERENCES

[1] D. K. Weaver, "A Third Method of Generation and Detection of Single-Sideband Signals," *Proc. IRE*, vol. 44, no. 12, pp. 1703-1705, Dec. 1956.

[2] F. Chastellain, C. Botteron, and P Farine, "Looking Inside Modern Receivers," *IEEE Microwave Magazine*, pp. 87-98, Apr. 2011.

[3] S. Wu and B. Razavi, "A 900-MHz/1.8-GHz CMOS Receiver for Dual-Band Applications," *IEEE Journal of Solid-State Circuits*, vol 35, no. 12, pp 2178-2185, Dec 1998.

[4] H. Hashemi and A. Hajimiri, "Concurrent Multiband Low-Noise Amplifier – Theory, Design, and Applications," *IEEE Transactions on Microwave Theory and Techniques*, vol. 50, no. 1, pp 288-301, Jan. 2002

[5] IRIG Standard 106-11, Chapter 2: Transmitter and Receiver Systems, June 2011

[6] M. Valkama, M. Renfors, and V. Koivunen, "Advanced Methods for I/Q Imbalance Compensation in Communication Receivers," IEEE *Transaction on Signal Processing*, vol. 59, no. 10, pp 2335-2344, Oct. 2001.

[7] J. P. F. Glas and M. W. Liao, "Digital I/Q Imbalance Compensation in a Low-IF Receiver," *Proc. IEEE Globecom*, pp. 1461-1466, Nov. 1998.